ANNALS OF GEOPHYSICS, 68, 2, NH215, 2025; doi:10.4401/ag-9178
OPEN ACCESS

Comparative Declustering Approaches for Seismic Data: Insights from Gardner-Knopoff, Gruenthal, Reasenberg, and Uhrhammer in the Kathmandu Valley

Dibyashree Poudyal[*,1], Norhaiza Nordin[1], Siti Nur Aliaa Roslan[2]

(1) Department of Civil Engineering, Infrastructure University Kuala Lumpur, De Centrum City, Jalan Ikram-Uniten, 43000 Kajang, Selangor, Malaysia
(2) Department of Civil Engineering, University Putra Malaysia, 43400 Serdang, Selangor, Malaysia

Article history: received October 2, 2024; accepted February 26, 2025

Abstract

Declustering is a crucial process that filters out dependent events to focus on independent mainshocks, thereby improving the accuracy of seismic hazard analysis. This study analyzes the spatiotemporal features of background seismicity in the Kathmandu Valley, Nepal using four widely applied declustering methods: Gardner and Knopoff, Gruenthal, Uhrhammer, and Reasenberg. A total of 3190 events from 2000 to 2023 that was analyzed using ZMAP software, revealing significant differences in the performance of each method. Statistical tools including the Allan factor, coefficient of variation Morisita index, and the inhomogeneous L-function were employed to assess spatial clustering, and temporal clustering behaviour. The results indicate that clustering persists in all declustered catalogs, with Reasenberg exhibiting the highest residual temporal clustering and Gruenthal the lowest. Spatial clustering analysis using the Morisita index revealed that Uhrhammer retained the strongest clustering, whereas Gruenthal produced the most homogeneous spatial distribution. Furthermore, L-function analysis with Monte Carlo simulations demonstrated that none of the declustered catalogs fully adhered to a homogeneous Poisson process, as all methods yielded p-values of zero. These findings underscore the limitations of current declustering techniques in completely removing clustering effects, emphasizing the need for refined methodologies in seismic hazard analysis. Future research should explore alternative declustering strategies and statistical models to better represent earthquake sequences in tectonically active regions like the Kathmandu Valley.

Keywords: Allan factor; Coefficient of variation; Declustering; L function; Morisita index

1. Introduction

Earthquake seismology bridges geology and geophysics, with earthquake catalogs providing crucial data such as epicenters, magnitudes, depths, and wave phases, which are essential for understanding the interior of the Earth. Seismologists, geophysicists, and geologists rely on this data, derived from seismic waves, to analyze subsurface

features and predict earthquake scenarios. Understanding seismicity patterns is vital for long-term forecasting and seismic hazard assessments, where earthquake data needs to be organized meaningfully, either as clustered or declustered events. Earthquakes are inherently linked to spatial and temporal phenomena, as described by the empirical Omori-Utsu relation (Utsu et al., 1995). However, earthquake databases often contain duplicate events, aftershocks, and foreshocks, which can distort hazard assessments. The initial step in conducting a seismic hazard analysis is to identify and validate the mainshock of the earthquakes. Declustering is a crucial process that filters out these dependent events to focus on independent mainshocks, improving the accuracy of seismic hazard analysis (Pramono et al., 2020). Several declustering methods have been developed, with the most commonly used ones being based on time-space windows, such as those by Uhrhammer (1986), Gardner-Knopoff (1974), Gruenthal and Reasenberg (1985). These methods allow for a more refined earthquake catalog, essential for hazard assessments.

The studies on declustering methods offer a comparative view of their effectiveness across various regions and datasets. Amini (2014) compares the Reasenberg and Gruenthal methods for northern Iran, showing that Reasenberg retains more seismic events, while Gruenthal produces a more conservative dataset. Risanti et al. (2022) analyze seismicity in Indonesia using Gardner and Knopoff, Reasenberg, and Uhrhammer, with techniques implemented in the software ZMAP finding Reasenberg most effective for regional seismicity characterization. In contrast, Van Stiphout et al. (2012) emphasize the importance of parameter selection in applying these methods, highlighting potential inaccuracies if not carefully chosen. Juellyan et al. (2023) find Uhrhammer the most effective for high-risk seismic evaluations, while Khurram and Khalid (2022) observe that Gardner and Knopoff identify a higher percentage of declustered events compared to Uhrhammer. Ansari et al. (2022) support Uhrhammer high declustering rate and effective separation of mainshocks. Few studies of probabilistic seismic hazard analysis conducted so far in Nepal, the Gardner and Knopoff algorithm declustering method has been used (Moklesur et al., 2018; Rahman et al., 2018; Bhusal and Parajuli, 2019; Pradhan et al., 2020; Parajuli et al., 2021). In seismically active regions like Kathmandu Valley, where the two Indian and Eurasian plates converge, selecting the right declustering method is critical for reliable seismic hazard analysis. Inaccurate data, such as heterogeneous magnitude distributions mapped

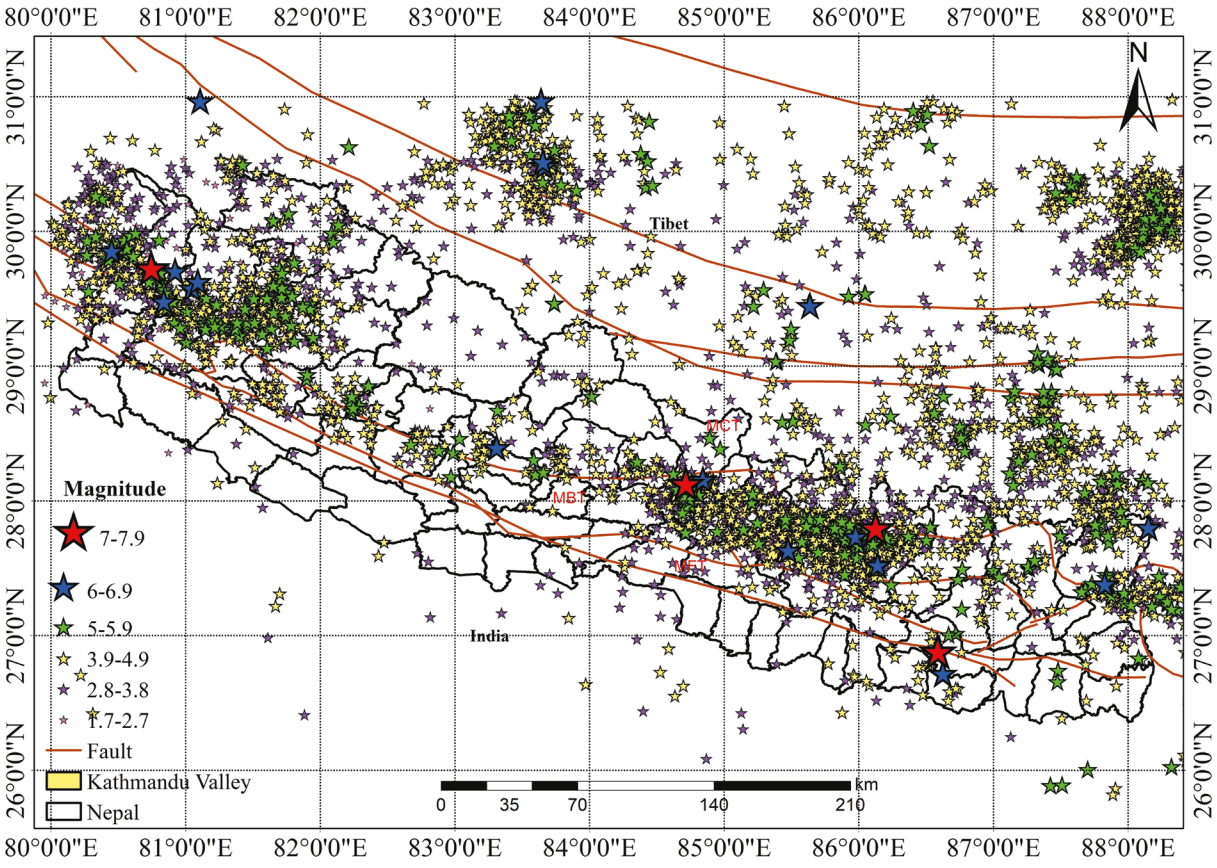

Figure 1. Seismicity distribution in and around Kathmandu Valley, Nepal.

in ArcGIS (Fig. 1 from the year 1916 to 2023) or erroneous depth estimations, can lead to flawed research outcomes (Teng and Baker, 2019).

Tools like ZMAP, a MATLAB-based graphical user interface, are often used to analyze earthquake source parameters and visualize seismicity distributions (Wiemer, 2001). This study focuses on the Kathmandu Valley, where the Indian and Eurasian plates converge, making it highly seismically active and necessitating accurate seismic hazard analysis. Given the challenges posed by heterogeneous magnitude distributions and depth estimation errors (Teng and Baker, 2019), this paper compares four widely-used declustering methods: Reasenberg (1985), Uhrhammer, Gruenthal, and Gardner-Knopoff (1974) considering the earthquake catalog between 1970 and 2023. By assessing the effectiveness of these methods in isolating mainshock events, this paper aims to identify which method is better suited for enhancing seismic hazard predictions based on the magnitude of completeness and seismicity parameters, such as the a and b values, in this highly seismically active region. The structure of the paper is as follows: Section 2 describes the overview of the earthquake catalog and its characteristics. Sections 3 and 4 describe the methodology and the tools used, Section 5 presents the results, and discusses the findings of the declustering analysis and their implications for seismic hazard assessments in the Kathmandu Valley. Finally, Section 6 concludes the study.

1.1 Seismotectonic setup of Kathmandu Valley

The Kathmandu Valley lies within a seismically active region at the boundary of the Indian and Eurasian tectonic plates. This collision generates frequent seismic activity, including both shallow and deep earthquakes. The proximity of Valley to the Main Himalayan Thrust (MHT) makes it particularly vulnerable to large seismic events. Historical records indicate significant earthquakes in 1833, 1866, 1934, 1988, and 2015 A.D. (Poudyal et al., 2024). The 1934 Nepal-Bihar earthquake, with an estimated magnitude of 8.0, was among the most devastating, causing widespread destruction in Kathmandu and neighboring regions in Bihar and India. This event claimed thousands of lives and significantly damaged infrastructure and historical sites. Similarly, the 2015 Gorkha Earthquake (M_w 7.8) caused extensive destruction, with 9,000 fatalities, over 21,000 injuries, and severe damage to 600,000 homes and public infrastructure. The most significant aftershock (M_w 7.3) on May 12, 2015, exacerbated the damage, particularly in areas already affected by the mainshock. Between 2019 and 2023, Nepal experienced three notable earthquakes, each causing varying degrees of destruction. In 2019, Thalara in Bajhang District was struck by a 5.1(M_w) earthquake, resulting in 153 deaths, 375 injuries, and the destruction of 200 houses. The 2022 earthquake in Doti, with a magnitude of 5.7(M_w), led to six fatalities, 12 injuries, and extensive property damage, with 924 houses collapsing and 5,186 others being damaged. The November 2023 earthquake in Jajarkot, Nepal, caused widespread devastation, leaving a significant impact on lives and infrastructure. At least 153 people, including many children, lost their lives, and nearly 400 individuals sustained injuries. The earthquake inflicted severe damage to buildings, with over half of the structures in Jajarkot. Across five impacted districts (Rolpa, Dolpa, Salyan, Rukum, and Jajarkot), a total of 61,964 houses were reported damaged, highlighting the extensive scale of destruction and the challenges faced by the affected communities. The Kathmandu Valley too experienced the shaking of these strong earthquakes.

1.2 Station Networks in Kathmandu Valley

The seismic network in Nepal, including those covering the Kathmandu Valley, plays a crucial role in monitoring and understanding the seismicity of the region. The National Seismological Centre (NSC) of Nepal operates a network of seismic stations that provides real-time data on seismic events. Additionally, several international networks, such as those managed by IRIS (Incorporated Research Institutions for Seismology) and USGS (United States Geological Survey), also contribute to earthquake monitoring in the region. The stations are distributed across Nepal, with a concentration in the Kathmandu Valley due to its high population density and seismic hazard. The seismic catalog analyzed in this study was compiled using data from multiple seismic station networks, including those from mentioned specific networks like the National Seismological Centre of Nepal (NSC), and other international collaborations. These networks provide crucial real-time data on seismic events and are distributed across various regions, allowing for the detailed monitoring of seismic activity in the Kathmandu Valley.

2. Earthquake Catalog and its characteristics

An earthquake catalog is a systematically compiled database of seismic events, detailing their occurrence times, epicenters, depths, and magnitudes. It serves as a foundational dataset for understanding seismicity patterns, assessing seismic hazards, and analyzing earthquake source parameters.The dataset used for declustering analysis exhibits notable heterogeneity, particularly in the earlier periods of the catalog. Significant gaps in the record before 1970 are characterized by long inter-event times and a lack of medium-to-low magnitude events. This incomplete representation of seismicity introduces artifacts that may skew the declustering results. Specifically, the absence of smaller earthquakes during the first half of the 20th century results in misleading long inter-event times, which do not reflect the true seismic activity. These gaps indicate that the catalog before 1970 is not homogeneous, making it unsuitable for robust declustering analysis. Furthermore, the heterogeneity is further emphasized when considering the distribution of events after 2000, where the frequency of earthquakes increases, and the time intervals between successive events become much shorter. The combination of missing events in the earlier years and the uneven distribution of events over time contributes to a heterogeneous dataset, potentially compromising the accuracy of the statistical results. To ensure a more reliable and homogeneous dataset for declustering a comprehensive earthquake catalog was compiled, including information on the focal depth, magnitude, depth, and timing of over 3190 seismic events from the year 2000 to 2023 with magnitudes ranging from 1.7 to 7.9 shown in Fig. 1, sourced from various online databases as tabulated in Table 1.

Seismological Centers	Online platforms
US Geological Survey (USGS)	https://earthquake.usgs.gov
International Seismological Centre (ISC)	http://www.isc.ac.uk/iscbulletin/search/catalog/
Integrated Research Institutes for Seismology (IRIS)	https://ds.iris.edu/ds/nodes/dmc/data/types/events/catalogs/
National Seismological Centre(NSC)	https://www.seismonepal.gov.np

Table 1. Data from online platforms.

The magnitudes available from the four different sources were surface-wave magnitude (M_s), local magnitude (M_l), and body-wave magnitude (M_b), all the magnitudes were homogenized into moment magnitude (M_w) using global empirical relationships to ensure uniformity across the catalog. These relationships for converting M_s to M_w, M_b to M_w, and M_l to M_w were adopted from Das et al. (2012). The resulting event catalogs were further input into the ZMAP software to analyze the effect of each procedure on the raw earthquake catalogs. ZMAP tool developed by Max Wyss, Stefan Wiemer, and Ramon Zuniga was used for this analysis (Wyss et al. 2001). The homogenized catalog is imported into ZMAP with earthquake events and the associated information arranged in the format of an ASCII file. In the Gardner-Knopoff method, which identifies aftershocks and foreshocks based on predefined time and distance windows, depth data is not explicitly considered; this method primarily focuses on epicentral distances. Similarly, the Uhrhammer method, which also uses fixed spatial and temporal windows, does not emphasize depth data and typically relies on epicentral distances. However, in the Reasenberg method, depth plays a more critical role as it calculates spatial distances using both horizontal and vertical (depth) components. This method evaluates clusters of seismic events by considering their three-dimensional spatial and temporal relationships, making depth an integral part of the clustering process. In addition to these methods, the Grüenthal declustering algorithm offers a distinct approach by incorporating magnitude-dependent spatial and temporal windows to identify foreshocks and aftershocks. Unlike the Gardner-Knopoff and Uhrhammer methods, which use fixed parameters, the Gruenthal method adjusts the clustering criteria dynamically based on the size of the earthquake event. Approximately 2.3 % of the entries in the catalog had missing depth values that were set to “10 km”. To address the potential

influence of missing data on the results, a sensitivity analysis was conducted by assigning missing depth values to “5 km”, “10 km”, and “15 km”. The results showed that the number of declustered events varied only slightly across these depth values for all methods. For instance, the Gruenthal resulted in 1172, 1173, and 1172 events when missing depths were set to “5 km”, “10 km”, and “15 km”, respectively. Similarly, the Reasenberg method produced 1020, 1040, and 1057 events, while the Gardner-Knopoff method resulted in 14676, 1466, and 1467 events. Lastly, the Uhrhammer method yielded 1767, 1770, and 1767 events across the same depth assignments. This indicates that the declustering process with a “10 km” default depth avoids overestimating or underestimating the number of mainshock and aftershock classifications, providing a more conservative and robust result. Moreover, assigning a depth of “10 km” aligns with the natural depth distribution in the catalog, where most earthquakes are concentrated at shallow depths with a peak at “10-20 km”.

2.1 Magnitude as a function of Depth

In general, larger seismic events tend to occur at shallow depths, while deeper earthquakes rarely occur beyond 200 km. The majority of earthquake events are concentrated at shallow depths, within the range of 0-20km, particularly around latitudes 25° to 30° and longitudes 80° to 90° with magnitudes ranging from 3 to 5. A notable cluster of earthquakes with magnitudes around 4 and 5 occurs at these shallow depths, indicating a high frequency of moderate-magnitude events. As depth increases beyond 40 km, both the number of earthquakes and their magnitudes decrease, showing a tapering effect as depicted in Fig. 2. The deeper earthquakes, particularly beyond 80 km, tend to have lower magnitudes, suggesting that large-magnitude events are uncommon at greater depths.

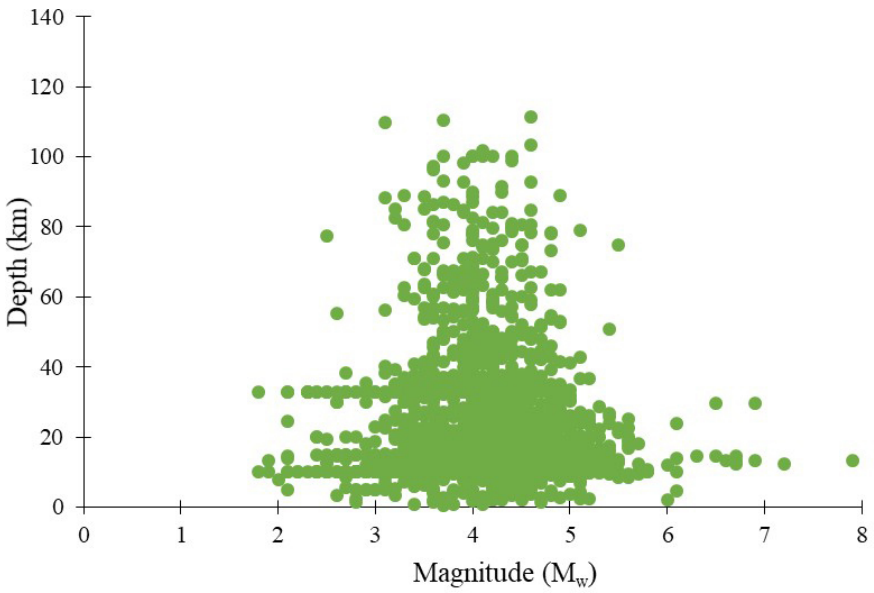

Figure 2. Magnitude as a function of Depth.

2.2 Seismic events as a function of depth, magnitude, period and event number

The earthquake catalog is widely recognized for containing extensive information. Figure 3 illustrates the relationships between various parameters. Figure 3a shows that most earthquakes occur at shallow depths primarily less than 50 km, with a significant peak at around 10-20 km. The frequency of events rapidly decreases beyond 50 km, indicating that deep-focus earthquakes are less common. The histogram of fig.3b indicates that most events have magnitudes concentrated between 3 and 5, with a peak at approximately magnitude 4. Larger magnitude earthquakes (above magnitude 6) are relatively rare in the dataset, while very small magnitude events (below 3) are also infrequent. Figure 3c shows the temporal distribution of events from 2000 onward. The data remain relatively

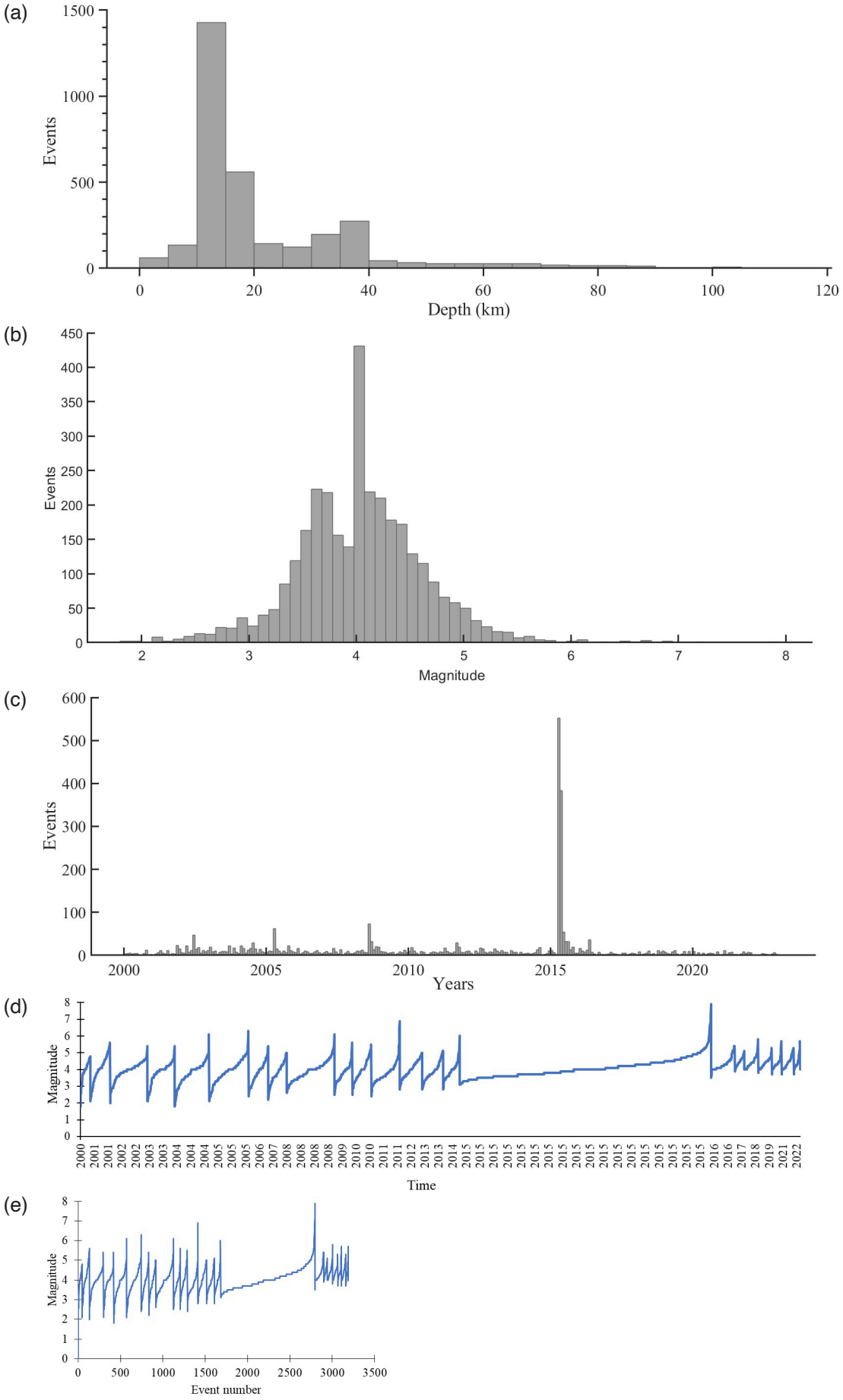

Figure 3. Seismic events as a Function of Magnitude, Depth, time and event number.

stable over time with minor fluctuations. However, a significant, spike was observed in 2015, likely due to the Gorkha earthquake and its aftershock sequence. This suggests that the increase in recorded events during that period is not due to gradual improvements in detection technology or catalog completeness but rather to a major seismic event. The lack of a consistent upward trend before and after 2015 further supports this interpretation, indicating that variations in recorded events are primarily driven by significant earthquakes rather than long-term changes in monitoring capabilities. Furthermore, to evaluate the completeness and homogeneity of the dataset, two graphical representations were used: (i) Time vs. Magnitude and (ii) Event Number vs. Magnitude. Figure 3d illustrates the temporal evolution of earthquake magnitudes, providing insights into data gaps or changes in recording practices. Before 2014, a relatively stable trend was observed, whereas a noticeable shift occurred after 2014, with an increase in recorded magnitudes around 2016. This may indicate either an actual increase in seismic activity or an artifact of improved data collection. Figure 3e further verifies data consistency by assigning a sequential event index. Initially, magnitudes appear consistently distributed, but after event number ~2500, a shift in magnitude patterns is evident.

3. Declustering methods

Seismic declustering plays a vital role in seismic hazard analysis to separate independent events (mainshocks) from aftershocks and foreshocks. Several methods have been developed to achieve this, each using different criteria based on temporal and spatial characteristics of earthquake events. In this section four declustering methods, comprising three window-based approaches by Gardner and Knopoff, Uhrhammer and Gruenthal, and the cluster-based method by Reasenberg, are discussed.

3.1 Windows-Based Declustering Method

Window-based declustering methods establish a space-time window for each seismic event based on its magnitude M, where the spatial and temporal dimensions of the window are functions of M. If a less significant earthquake occurs before a higher-intensity earthquake within the same window, the window is adjusted to center on the event with the greater magnitude. The significant earthquake within the adjusted space-time window is designated as the mainshock and included in the declustered catalog, while all other events within the window are excluded. The current analysis compares space-time window sizes of methods: Gruenthal, Gardner and Knopoff, and Uhrhammer as implemented and available in ZMap software. Among the simplest window-based methods for identifying aftershocks and mainshocks is the method proposed by Gardner and Knopoff. Following an earthquake, all additional seismic events that occur within particular time and space frames are classified as aftershocks, with these windows typically being functions of the mainshock magnitude which is the greatest earthquake in the cluster. Seismic events of lesser magnitude that occur before the mainshock are considered foreshocks. However, this method does not account for secondary or higher-order aftershocks, which are triggered by previous aftershocks. Additionally, the space window in this method is assumed to be circular, affecting the distribution of aftershocks. A representation of the window sizes as described by Gardner and Knopoff can be represented as shown:

$$t = \begin{cases} 10^{0.032M+2.7389} & \text{if } M \geq 6.5 \\ 10^{0.5409M-0.547} & \text{if } M < 6.5 \end{cases} \quad (1)$$

$$d = 10^{0.1238M+0.983} \quad (2)$$

where, d denotes the distance in km, t represents the temporal window of seismic events and M represents the magnitude of the mainshock.

The Uhrhammer method is one of several declustering techniques that use different physical and statistical assumptions. It is a systematic approach to distinguish dependent seismic events, such as aftershocks and foreshocks, from mainshocks in an earthquake catalog. The method uses temporal, spatial, and magnitude criteria to classify events. A key feature of the method is its reliance on magnitude-dependent relationships to define the time or

spatial window, reflecting the observation that larger earthquakes tend to produce aftershocks over longer times and greater distances. This method uses the following equations:

$$t = e^{-2.87+1.235M} \tag{3}$$

$$d = e^{-1.024+0.804M} \tag{4}$$

The Gruenthal declustering method is a widely used approach to separate earthquake sequences into mainshocks and dependent events, such as aftershocks and foreshocks. It operates by defining space-time windows around each earthquake, with the size of these windows determined as a function of the earthquake's magnitude. Larger earthquakes influence a broader spatial and temporal range; these empirically calibrated windows help identify dependent events. A key feature of the method is its dynamic adjustment of space-time windows: When a lower-intensity earthquake is followed by a more significant event within the defined window, the window is recalculated based on the larger event, which is then classified as the mainshock. All other events within this updated window are considered dependent and are removed from the catalog. The space-time window sizes used in this study are defined by the following relationships:

$$t = \left|e^{-3.95+(0.62+17.32*M)^2}\right| \text{ if } M \geq 6.5 \tag{5}$$

$$t = e^{2.88+0.024*M} \text{ if } M < 6.5 \tag{6}$$

$$d = e^{1.77+(0.037+1.02M)^2} \tag{7}$$

where, d is the distance (km), t is the time (days), and M is the earthquake magnitude.

3.2 Clustered-Based Method

The Reasenberg (1985) method associates earthquakes occurring within a defined space-time interaction zone and organizes them into aftershock clusters. In this approach, if earthquake P is an aftershock of Q, and Q is an aftershock of R, all three events (P, Q, and R) are grouped in the same cluster of aftershock. This ensures that subsequent and higher-order aftershocks are accounted for in the analysis. The largest earthquake within a cluster is designated as the mainshock. The time-dependent interaction zone is defined by Omori's law, which describes the decay rates of aftershock activity, while the spatial influence zone is determined by the extent of the seismic source. The connection between isolated events and grouped seismic events is governed by their temporal and spatial interaction dynamics. The relationship of time interaction is characterized through the ensuing Eq. (8):

$$\text{LogD(km)} = 0.4M - 1.943 + k \tag{8}$$

where, D denotes the spatial threshold, measured in kilometers; M refers to the earthquake's magnitude; k represents the spatial proximity parameter. The relationship for time dependent interaction is expressed as:

$$\tau = -\ln(1 - p_1) * t/10^{2(\Delta M-1)/3} \tag{9}$$

τ denotes the time limit; t is the present time; p_1 indicates the likelihood of identifying the subsequent cluster event, ΔM is the variation between the maximum earthquake magnitude and the threshold magnitude, $\Delta M = M - x_{meff}$ with M being is the magnitude of mainshock and x_{meff} referring to the minimum magnitude cutoff for the earthquake catalog.

4. Statical Metrics for Spatiotemporal Analysis of Background Seismic Events

This section outlines various statistical methods used to analyze the space-time characteristics of background earthquake occurrences. Five statistical tools are introduced: Coefficient of variation, Allan factor, Morisita indexand the inhomogeneous L-function.This analysis follows the procedure proposed in Benali et al. (2023) for spatio-temporal analysis of background seismicity.

4.1 Coefficient of Variation

The Coefficient of Variation (CV), expressed as the ratio of the standard deviation $\sigma(t)$ to the mean of intervals among successive seismic events, is a widely used metric for assessing clustering behavior in earthquake sequences. The relationship used for CV is as shown below:

$$CV = \frac{\sigma(t)}{Mean(t)} \tag{10}$$

When the Mean(t) equals the standard deviation ($\sigma(t)$ in a Poisson process, the CV is 1. A clustered process has a CV greater than 1 when $\sigma(\tau) > Mean(t)$. The time scales over which the process displays clustered or Poissonian behavior, however, is not shown by this coefficient. The following empirical measure can be used to explore Poissonian behavior further.

$$Y(t) = \frac{N(t)}{\sqrt{\lambda t}} - \sqrt{\lambda t} \tag{11}$$

where λ represents the rate of a homogeneous Poisson process over time and N(t) denotes the cumulative number of events in the catalog up to time t. Assuming a homogeneous Poisson process, Y(t) has a mean of zero and a variance of one. Monte Carlo simulations are conducted to generate confidence bands for Y(t) based on assumption to compare these bands with the observed Y(t).

4.2 Allan Factor

The Allan Factor (AF) is a tool to analyze the occurrence of clustering patterns in earthquakes, which represent an instance of a temporal point process. The time axis is divided into equal-length intervals of size t with N_k representing the number of events in the k^{th} interval. N_k constitutes a discrete random process of nonnegative integers. The expression for Allan Factor (AF) is expressed as:

$$AF(t) = \frac{E\left[\left(N_{k+1}(t) - N_k(t)\right)^2\right]}{2E[N_K(t)]} \tag{12}$$

Here, E presents the expectation symbol. In a homogeneous Poisson process, AF(t) remains approximately equal to one across all timescales, producing a flat plot of AF(t) vs t. If $AF(t) > 1$, it indicates clustered behavior. For a fractal point process, AF(t) increases with t following a power-law relationship.

$$AF(t) = 1 + \left(\frac{t}{t_1}\right)^{\alpha} \tag{13}$$

where $0 < \alpha < 3$ is the fractal exponent quantifying clustering intensity, and t_1 is the fractal onset time that represents the minimal threshold beyond which the fractal behavior becomes observable.

4.3 Morisita Index

Morisita Index (I_δ) is employed to examine the spatial clustering behavior in earthquake patterns. Using a grid consisting of M cells with variable sizes δ Morisita is defined as follows:

$$I_\delta = M\frac{\sum_{i=1}^{M}(n_i - 1)\, n_i}{N(N-1)} \tag{16}$$

where n_i is the number of events within the i^{th} cell and N is the total number of seismic events. To create the plot correlating each I_δ to its equivalent δ, it is recommended, to begin with a relatively large cell size δ and iteratively reduce δ until a minimum value is achieved. I_δ fluctuates around 1 for Poissonian behavior and decreases toward zero for clustered behavior. Additionally, the Morisita slope S_2 is defined as the slope of the linear regression line that fits $\log_{10} I_\delta$ and $\log_{10}\delta$

$$\lim_{\delta \to +\infty} | \frac{\log_{10} I_\delta}{\log_{10}\delta} \approx S_2 \tag{17}$$

This slope, S_2, quantifies the indicates the clustering in the earthquake sequence: the larger the value of S_2, the higher the degree of clustering.

4.4 Inhomogeneous L Function

An inhomogeneous adaptation of Besag's L function is employed to assess whether the spatial distribution of earthquake epicenters aligns with a spatially inhomogeneous Poisson process characterized by a seismicity rate λ(x,y). The empirical L-function, derived as a transformation of Ripley's K-function, is defined as follows:

$$L(r) = \sqrt{\frac{K(r)}{\pi}} = \sqrt{\frac{1}{\pi}\sum_{i=1}^{N}\sum_{j\neq i=1}^{N} \frac{I\left\{(x_i - x_j)^2 + (y_i - y_j)^2 \le r^2\right\}}{\lambda(x_i, y_i)\lambda(x_j, y_j)\left|\mathcal{M}_i \cap \mathcal{M}_j\right|}}, \quad r \ge 0 \tag{18}$$

The indicator function I evaluates to 1 when a specified condition is valid and 0 otherwise. The K(r) function represents the expected value of the sum $1/\lambda\,(x_i, y_i)$ overall longitude x_i and latitude y_i pairs within a distance r. Here, $\mathcal{M}_i = \{(x - x_i, y - y_i) : (x, y) \in M\}$ is the translation of the geographical region $\mathcal{M}$ by (x_i, y_i) and $\left|\mathcal{M}_i \cap \mathcal{M}_j\right|$ represents the area of the intersection between $\mathcal{M}_i \cap \mathcal{M}_j$. For all distances $r \ge 0$, $L(r) = r$ for an inhomogeneous Poisson process with intensity function $\lambda\,(x, y)$. $L(r) < r$ indicates a negative correlation whereas $L(r) > r$ indicates positive correlation (clustering) at distance r.

5. Result and Discussion

The declustering analysis tabulated in Table 2 and the seismicity maps mapped in GIS for the region, presented in Fig. 4 derived from the four methods Gardner and Knopoff, Gruenthal, Uhrhammer, and Reasenberg, provide insight into their performance and impact on the earthquake catalog. In this context, the mainshock refers to the

largest event in a sequence, identified as the primary seismic event that triggers a series of aftershocks. The term cluster refers to a group of earthquakes, including the mainshock and its aftershocks, as this Reasenberg method identifies clusters of seismic events using spatial and temporal criteria.

Methods	Number of events	Main shock	Removed events (%)	Declustered events	M_c	a	b
Gardner and Knopoff	3190	116	1724(54.04%)	1466	4	5.194	0.91 ± 0.03
Reasenberg	3190	163	2150(27.49%)	2313	4	5.971	1.06 ± 0.03
Uhrhammer	3190	66	1420(44.51%	1770	4	5.444	0.95 ± 0.03
Gruenthal	3190	147	2017(63.22%)	1173	4	4.953	0.88 ± 0.03

Table 2. Results of different declustering methods from Zmap.

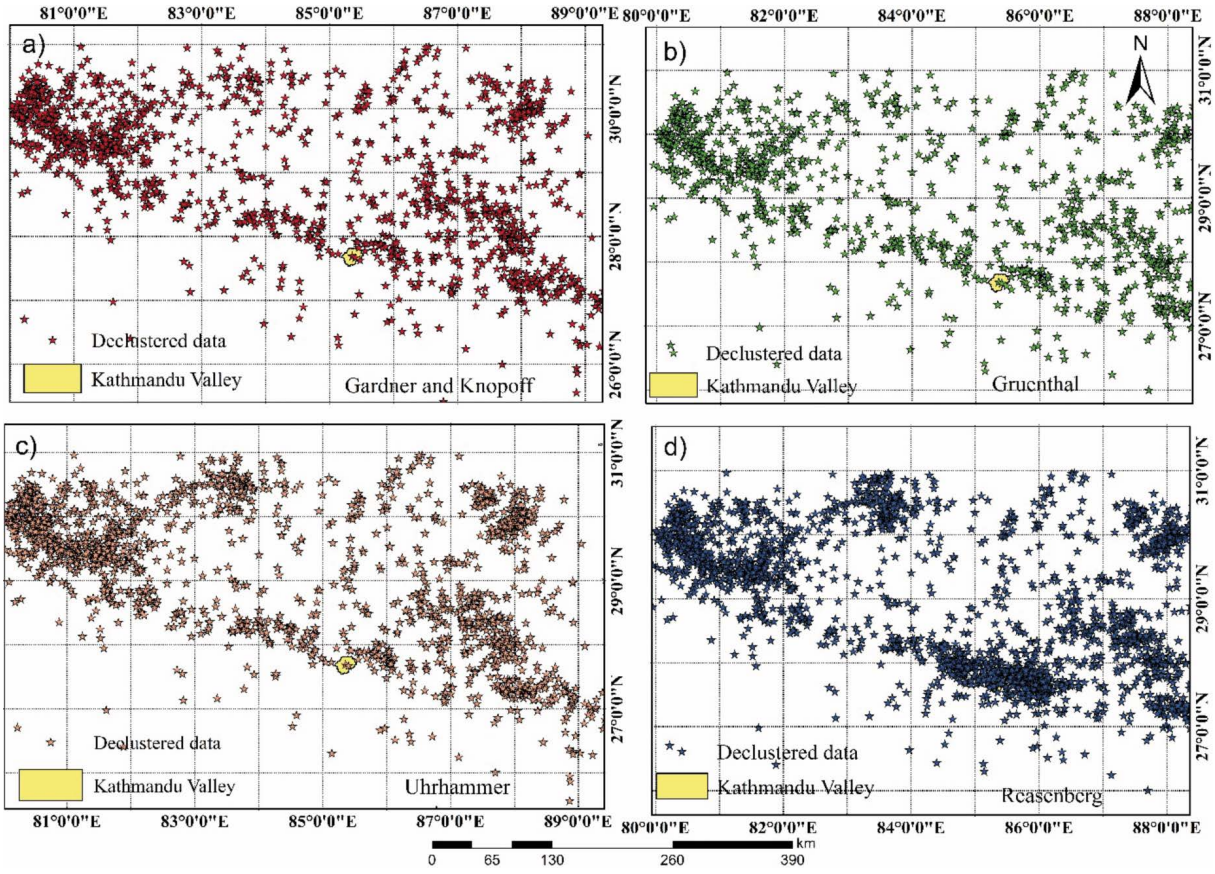

Figure 4. Declustered data from four different methods.

The analysis of the declustered earthquake events in Kathmandu Valley using the Gardner and Knopoff, Gruenthal, Uhrhammer, and Reasenberg methods reveals notable differences in their approaches and outcomes. Table 2 presents a comparative analysis of four declustering methods applied to an earthquake catalog consisting of 3,190 events. Reasenberg retains the highest number of declustered events (2313) and removes only 27.49% of the total events, indicating that it is the least restrictive method. In contrast, Gruenthal removes the highest percentage

of events (63.22%), leaving only 1173 declustered events, making it the most restrictive. Gardner and Knopoff and Uhrhammer fall between these two extremes, with Uhrhammer retaining 1770 declustered events and Gardner and Knopoff retaining 1466. Despite these differences, all methods maintain a consistent completeness magnitude of 4 (Fig. 5), ensuring a uniform lower magnitude threshold across the declustered datasets.The Gutenberg-Richter a-value, which represents the seismic activity rate, is highest for the Reasenberg method (5.971), suggesting

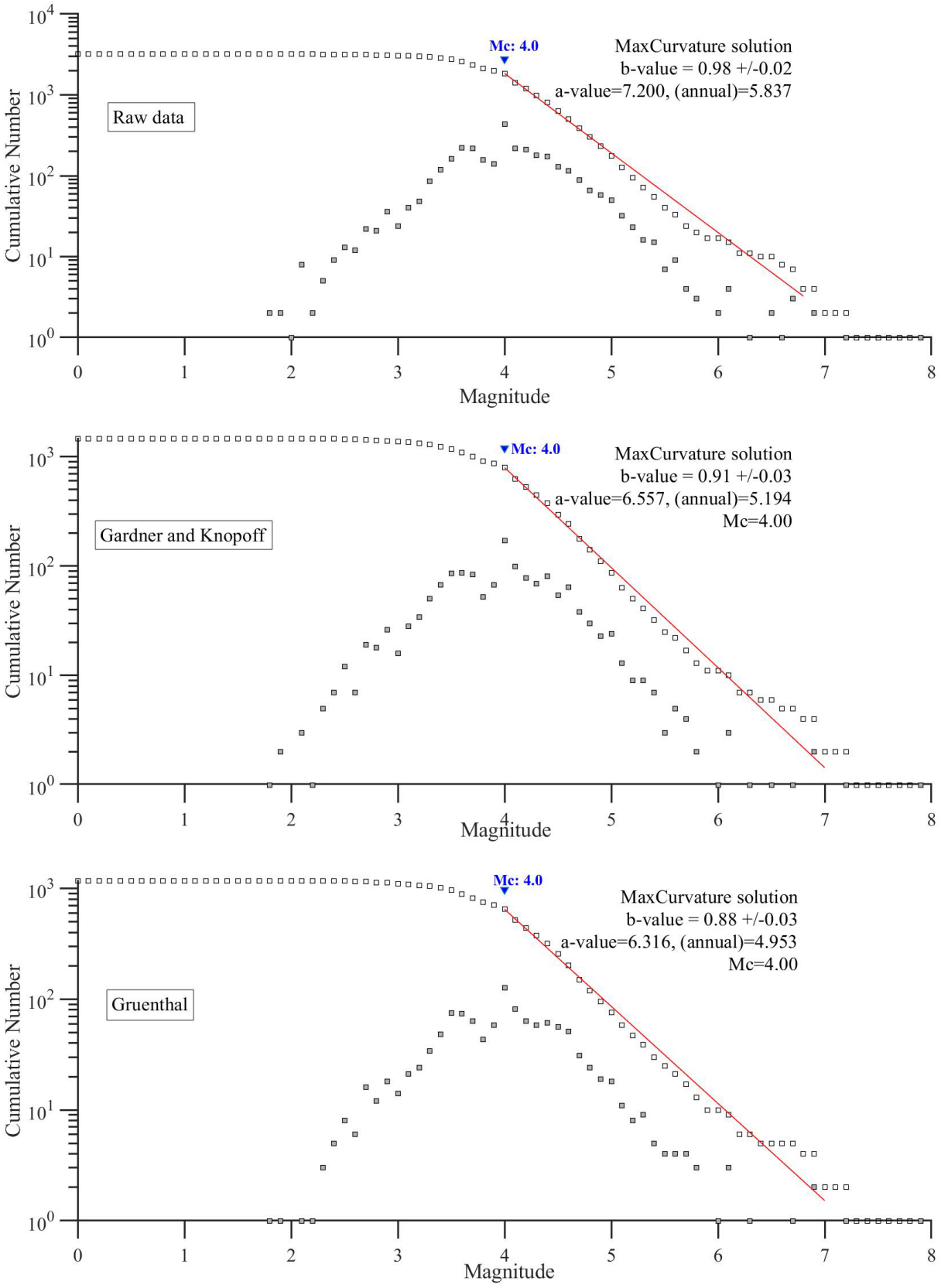

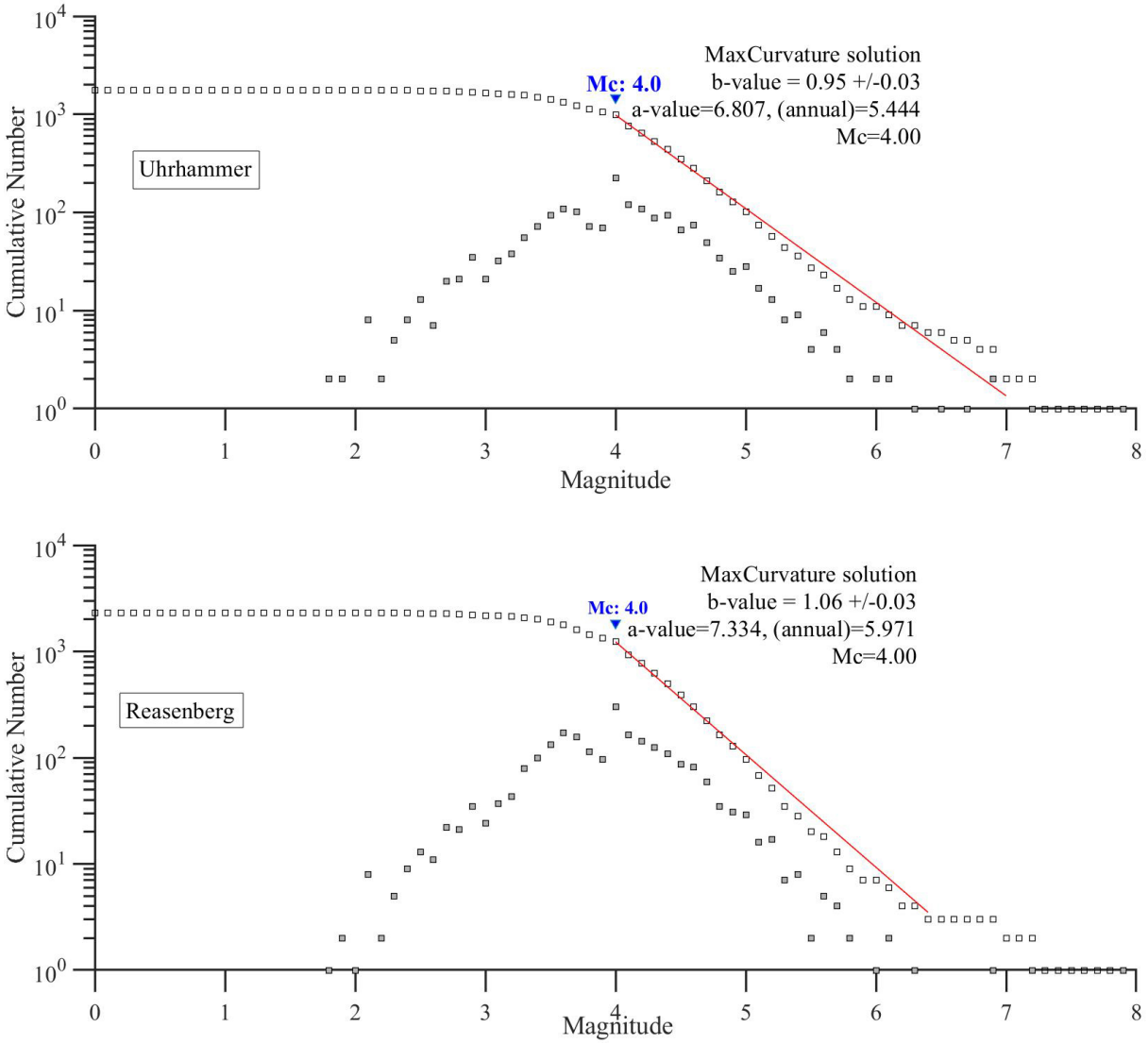

Figure 5. Comparison of Gutenberg-Richter relationships for the three declustering methods, showing the cumulative number of events versus magnitude and corresponding a and b values.

a higher frequency of earthquakes per unit area and time, while the Gruenthal method exhibits the lowest (4.953), indicating a comparatively lower seismicity rate. Similarly, the b-value, which characterizes the distribution of small and large earthquakes, is highest for Reasenberg (1.06 ± 0.03), reflecting a dataset dominated by small-magnitude earthquakes, whereas the Gruenthal method has the lowest (0.88 ± 0.03), indicating a relatively higher proportion of large-magnitude events. The Gardner-Knopoff (0.91 ± 0.03) and Uhrhammer (0.95 ± 0.03) methods fall in between these extremes.

The completeness of earthquake catalogs varies among the four declustering methods: Gruenthal, Reasenberg, Gardner and Knopoff, and Uhrhammer, as evident from their cumulative event plots across different magnitude ranges starting from 2000. For smaller magnitudes ($4.0 \leq M_w < 4.4$), all methods show reliable recording and completeness from 2000 onward, with Gruenthal and Uhrhammer exhibiting smoother and more consistent trends compared to Gardner and Reasenberg. In the moderate magnitude range ($4.5 \leq M_w < 4.9$ and $5.0 \leq M_w < 5.4$), Gruenthal shows stable cumulative growth, confirming completeness without significant gaps, while Uhrhammer and Reasenberg indicate slightly lower cumulative event counts, likely due to stricter filtering of dependent events. For magnitudes between 5.5 and 5.9, Gruenthal maintains a steady upward trend from 2000 without deviations, confirming completeness in this range, whereas Gardner and Reasenberg plots exhibit slight fluctuations. For larger magnitudes ($M_w \geq 6.0$), all methods show completeness despite fewer recorded events, reflecting the lower natural frequency of such events. Gruenthal's gradual and consistent cumulative trends across all magnitude

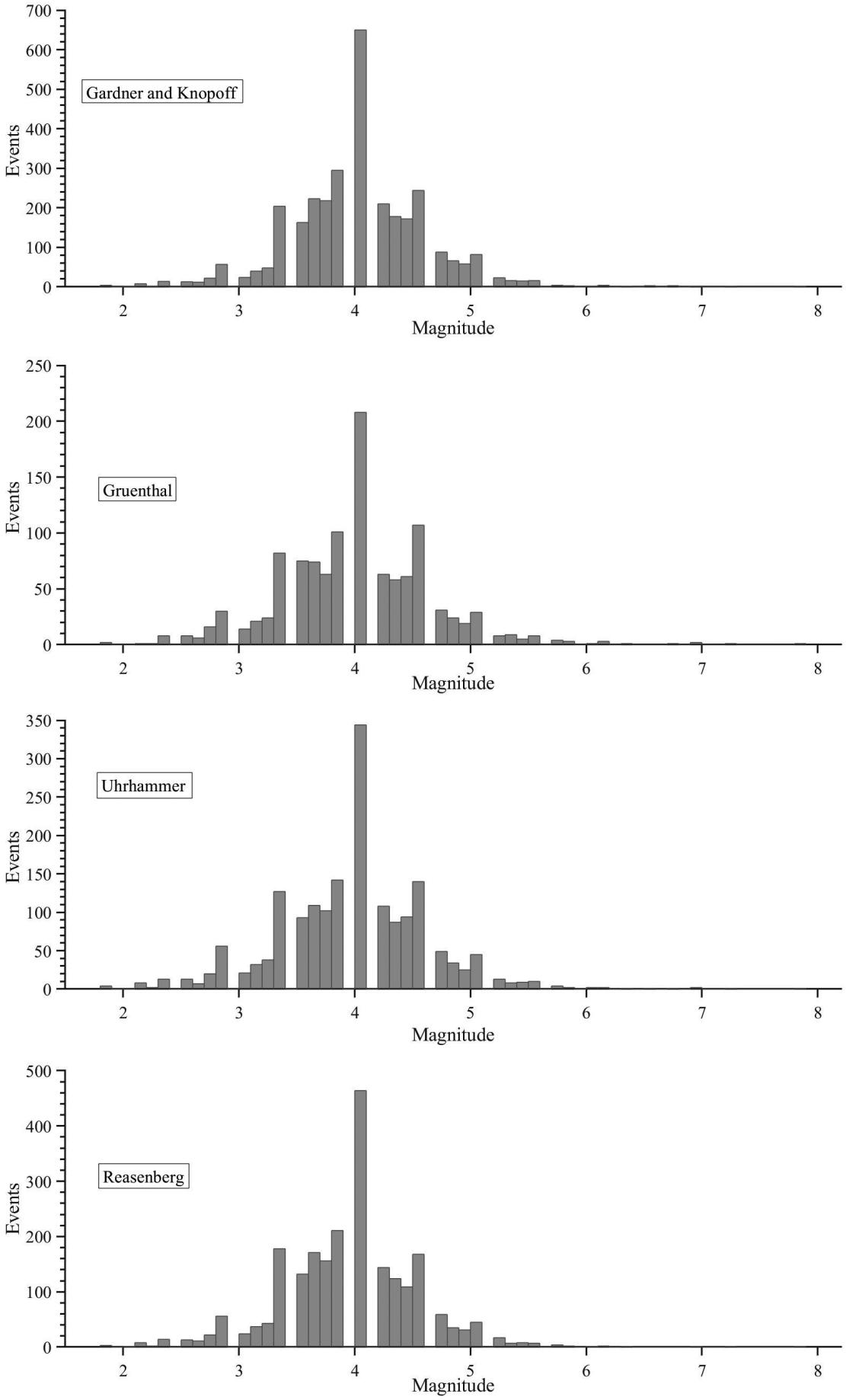

Figure 6. Magnitude histograms of Gardner Knopoff, Reasenberg, and Uhrhammer earthquake catalog.

ranges, particularly from M_w 4.5 and above, affirm a completeness magnitude (Mc) of 4.0, supporting its reliability for hazard assessment. This is because the characteristic-dependent earthquake varies according to region and therefore, various declustering methods have been proposed in various regions et al., 2012). Figure 6 illustrates the magnitude distributions of declustered seismic events for four declustering methods: Gardner and Knopoff, Gruenthal, Uhrhammer, and Reasenberg. The histograms, with a bin size of 0.1, highlight the differences in how each method filters and retains seismic events.

The magnitude histograms for the Gardner-Knopoff, Gruenthal, Reasenberg, and Uhrhammer earthquake catalogs reveal distinct patterns in the distribution of seismic events based on the declustering method used. The Gardner and Knopoff method retains a high number of events, with a distinct peak around magnitude 4.0, and a relatively symmetric distribution that gradually declines towards higher magnitudes. Similarly, the Reasenberg method also exhibits a peak near magnitude 4.0, maintaining a significant number of moderate-magnitude earthquakes while slightly reducing the number of smaller events compared to Gardner-Knopoff. On the other hand, the Uhrhammer method follows a comparable trend but removes more events, resulting in a lower total event count. The Gruenthal method appears to apply a stricter declustering approach, leading to a reduced number of events overall, with a more gradual spread of magnitudes. Across all methods, the dominance of magnitude 4.0 earthquakes is evident, while higher-magnitude events (above 6.0) are relatively scarce, as expected in the dataset. Similarly, Fig. 6 is supported by the statistics tabulated in Table 3, which provides the minimum, 10%, 25%,50%,75%, and 90% quantiles, a maximum, mean, and standard deviation of the magnitude sets.

Methods	Quantiles					Mean	Standard deviation	Maximum
	10%	25%	50%	75%	90%			
Gardner and Knopoff	3.2	3.5	4	4.4	4.7	3.96	0.669	7.9
Reasenberg	3.2	3.6	4	4.3	4.6	3.93	0.598	7.9
Uhrhammer	3.2	3.6	4	4.4	4.7	3.96	0.659	7.9
Gruenthal	3.2	3.6	4	4.4	4.8	3.99	0.672	7.9

Table 3. Summary statistics of magnitude sets for the four declustering methods.

Additionally, the number of earthquakes common across the declustered catalogs of all four methods is illustrated using a Venn diagram (Fig. 7), highlighting the intersection of this dataset. At the core of the diagram, 1,079 earthquakes are common to all four methods, representing the most robust events consistently identified across different approaches. Surrounding this core, several subsets highlight overlaps among three or two methods. Gardner-Knopoff, Uhrhammer, and Reasenberg share 275 events, while 306 events are common between Uhrhammer and Reasenberg alone. Other smaller intersections, such as 31 events shared by Reasenberg, Gruenthal, and Uhrhammer, indicate moderate variations in retained events. Each method also retains a set of unique earthquakes that are not identified by the others. Reasenberg shows the highest retention with 589 unique events, suggesting it the most inclusive approach, keeping more earthquakes in the catalog. In contrast, Gardner and Knopoff (10), Gruenthal (7), and Uhrhammer (30) retain significantly fewer unique events, implying a more selective approach in filtering dependent events. The large exclusive retention by Reasenberg highlights its tendency to preserve more events, while Gruenthal appears to be the most restrictive among the four methods.

The declustered catalogs were evaluated using various space-time empirical metrics to determine whether space-time clustering persisted to assess the hypothesis that a declustered catalog follows a temporally homogeneous but spatially inhomogeneous Poisson process. The coefficient of variation (CV) was applied to assess the clustering behavior, without focusing on specific timescale ranges where clustering was evident, including the empirical measure described in Eq. (11). Subsequently, the Allan factor was used to evaluate and quantify the time correlation

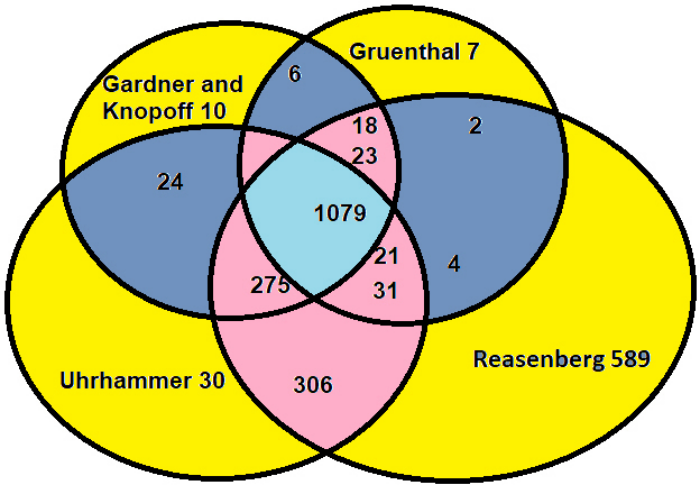

Figure 7. Veen Diagram showing the overlap of earthquake events identified as main shocks.

within the resulting background seismicity. A straightforward evaluation of the time-homogeneous Poisson hypothesis was conducted using the CV measure from Eq. (10), calculated for all declustered catalogs (Table 4).

Methods	Gardner and Knopoff	Gruenthal	Uhrhammer	Reasenberg
CV	1.32	1.29	1.45	1.69

Table 4. CV values of all declustered catalog.

The results showed CV values exceeding unity, indicating the potential presence of clustering behavior. Typically, a coefficient of variation significantly >1 suggests that clustered earthquakes continue clustering in the declustered catalogs, with the Reasenberg declustered catalog exhibiting greater clustering than the other catalogs. Among these, the Reasenberg declustered catalog exhibited the greatest clustering, while Gruenthal showed the lowest CV. Further statistical tests are required to determine whether the CV values are substantially different from one. Using Eq. (11), Figure 8 presents the Y(t) plots for all declustered catalogs, along with their equivalent 95% envelopes obtained from Monte Carlo simulations. The results revealed that none of the declustered catalogs were fully Poissonian across all timescales. In the Gardner and Knopoff, the observed curve starts near the lower confidence band, gradually rising before declining after around 7000 days, with noticeable deviations from the Poisson assumption during the growth phase but better alignment in later stages. The Gruenthal plot shows an initial upward trend closely following the theoretical curve, with mild fluctuations outside the confidence bands but eventual stabilization. Uhrhammer exhibits the best fit to the Poisson process, with smooth trends and minimal deviations that mostly remain within the confidence intervals, indicating strong compatibility with Poisson assumptions. The Reasenberg plot presents a distinct spike near 6000 days, where observed values sharply exceed the upper confidence bound before returning to alignment with the theoretical process and subsequently decaying. Overall, Uhrhammer demonstrates the closest fit to a Poisson process, while Reasenberg and Gardner-Knopoff show significant deviations, suggesting non-Poisson events or conditions.

Figure 9 illustrates the Allan factor (AF) curve (blue line) for each declustered catalog on a log-log scale, alongside the theoretical Poisson (green line) and the 95% confidence band derived through Monte Carlo simulations of a time-homogeneous Poisson process with an equivalent rate and event count to the original declustered catalog. The Gardner and Knopoff plot shows a gradual increase in the observed AF over time, with significant deviations beyond the confidence bounds, indicating non-Poisson behavior. Similarly, the Gruenthal model displays a steady rise in the observed AF with fluctuations, consistently exceeding the theoretical bounds. Uhrhammer exhibits

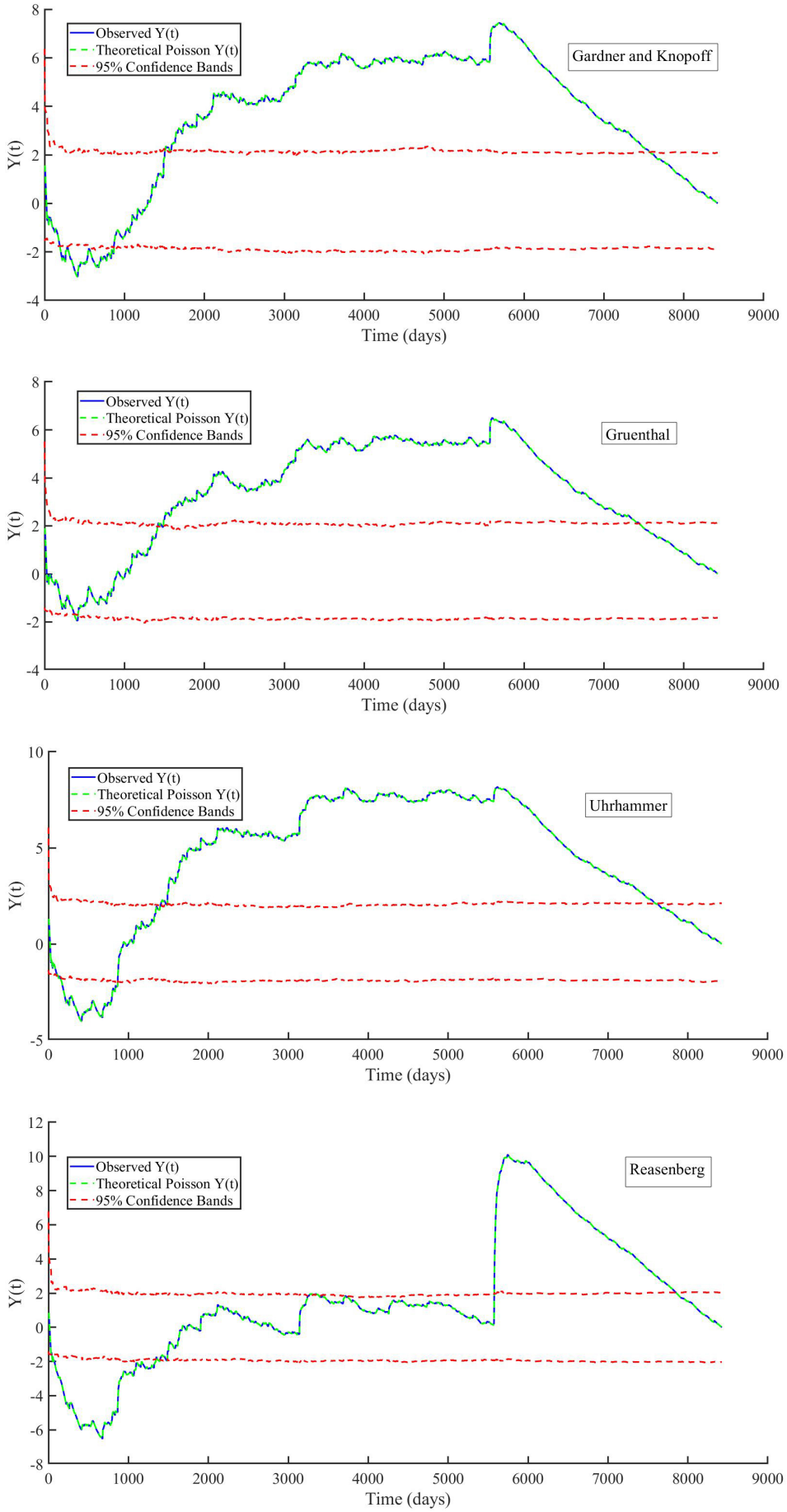

Figure 8. Theoretical, observed poisson with 95% confidence band of Y(t) for all declustered catalogs.

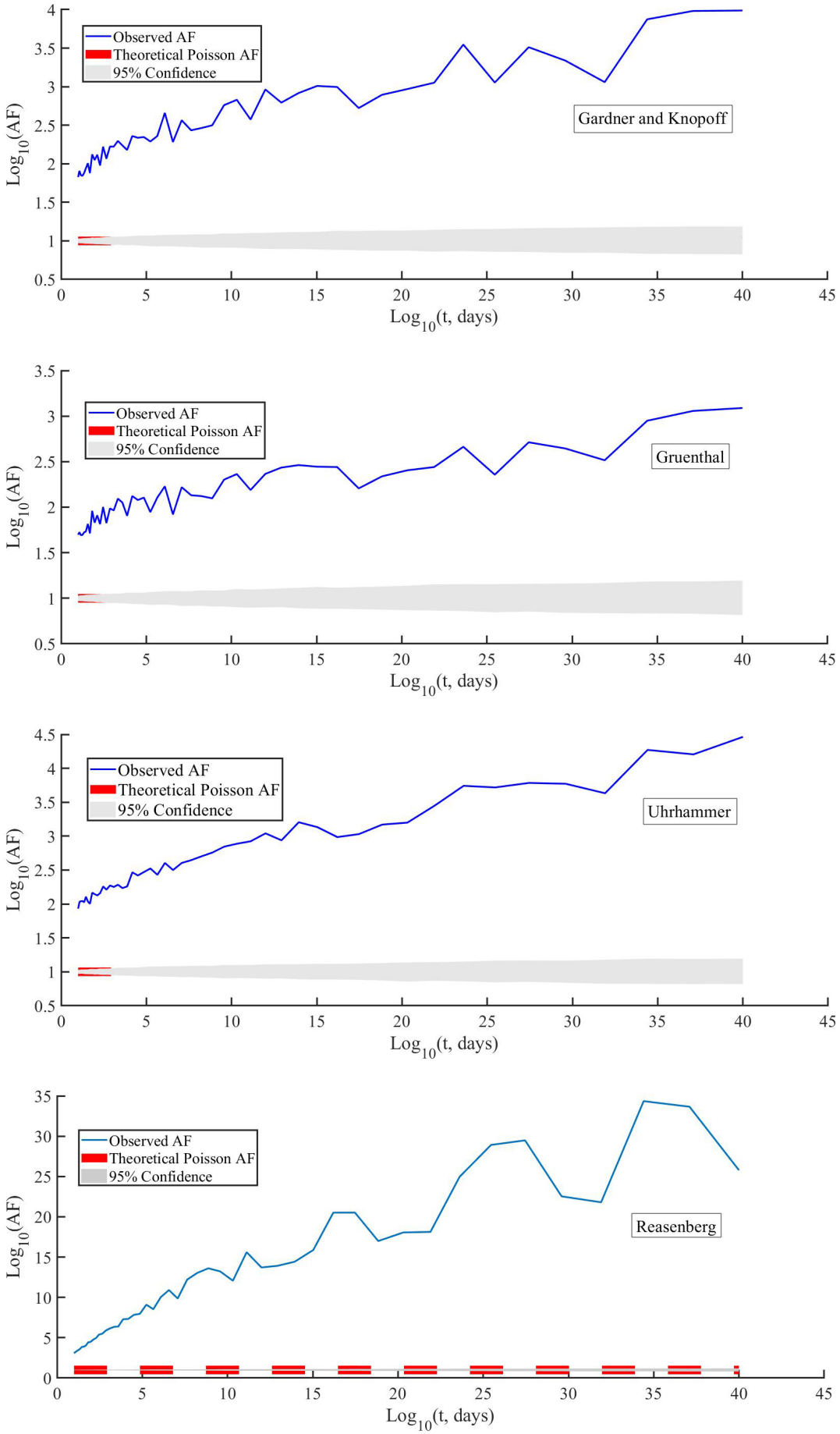

Figure 9. Log-log scale plots of Allan factor F with observed, theoretical, and 95%confidence area.

a smoother and more gradual trend, with better alignment between the observed and theoretical AF, suggesting stronger compatibility with the Poisson process compared to other models. In contrast, the Reasenberg model shows the most extreme deviations, with a sharp rise and significant departures from the theoretical Poisson AF, indicating highly non-Poisson behavior and potential bursts of activity.

The spatial characteristics of the four earthquake catalogs were analyzed using the Morsita index (I_δ) along with inhomogeneous L-function, as defined in Eq. (16) and (18), to assess spatial clustering. Figure 10 presents the linear regression of log10 I_δ against log10(δ), where I_δ represents the Morsita index value for a spatial grid with cell size δ. The S_2 slope of the Morisita index (I_δ) reflects the rate of change in clustering intensity for cell size, as observed in the bottom graphs of each method Each method displays unique clustering characteristics. The S_2 slope of the Morisita index (I_δ) reflects the rate of change in clustering intensity for cell size, as observed in the bottom graphs of each method. Each subplot includes the Morisita index across varying cell sizes (I_δ) in the top panels, along with log-log plots of log10 (I_δ) versus log10 (I_δ) in the bottom panels. The Gardner and Knopoff method shows a fluctuating Morisita index with notable peaks at higher cell sizes (around 5 and 9). The log-log plot reveals a moderate clustering behavior with a linear fit slope $S_2 = -0.22$. In contrast, the Gruenthal method exhibits relatively stable and lower Morisita index values, indicating weaker clustering. The empirical mean aligns closely with observed data, and the slope of the log-log plot ($S_2 = -0.19$) further confirms the minimal clustering. On the other hand, the Uhrhammer method displays significant fluctuations in the Morisita index, with prominent peaks near cell sizes 4 and 9. The steep decline in the scaling plot, characterized by a slope of $S_2 = -0.24$ indicates the strongest clustering behavior among the four methods. Similarly, the Reasenberg method shows irregular variations in the Morisita index, with peaks resembling those in the Uhrhammer model. Although the empirical mean closely follows the observed values, the slope ($S_2 = -0.21$) suggests moderate clustering, stronger than Gruenthal but weaker than Uhrhammer.

The inhomogeneous L-function results shown in Fig. 11 for the four declustering methods- Gardner and Knopoff, Gruenthal, Uhrhammer, and Reasenberg show clear differences in their ability to reduce spatial clustering in the background earthquake catalogs. In all cases, the empirical L(r) remains close to the x-axis, indicating that the spatial distribution of earthquake events is nearly homogeneous after declustering. The theoretical Poisson L(r) follows a linear increase with distance, serving as a reference for complete spatial randomness, while the confidence bands remain close to the empirical L(r), suggesting minimal clustering. Additionally, the p-value is zero for all declustering methods, indicating strong statistical evidence that the observed spatial distribution significantly deviates from a homogeneous Poisson process. Comparing the four methods, the results are quite similar, with slight variations. The Gruenthal and Reasenberg methods show almost identical behavior, implying that they remove clustered events similarly. The Gardner and Knopoff method appear to be slightly more aggressive in declustering, as its empirical L(r) deviates slightly more from the theoretical Poisson L(r). The Urhammer method follows a similar trend but seems to retain marginally more clustering compared to Gardner and Knopoff. However, since the p-value remains zero in all cases, it confirms that even after declustering, the spatial pattern still significantly deviates from a homogeneous Poisson process, suggesting that residual clustering or non-randomness remains in the data.

The results of this study indicate that clustering behavior persists in declustered earthquake catalogs, both temporally and spatially, consistent with the findings of Benali et al. In temporal clustering analysis, the coefficient of variation (CV) values for all declustered catalogs (Gardner and Knopoff: 1.32, Gruenthal: 1.29, Uhrhammer: 1.45, Reasenberg: 1.69) exceed unity, suggesting that earthquake sequences remain clustered even after declustering. Among the methods, Reasenberg exhibited the highest CV, indicating the strongest residual clustering, while Gruenthal showed the lowest, suggesting more homogeneous sequences. These trends align with Benali et al., who also observed that Reasenberg declustering retained significant clustering, whereas Gruenthal produced a more independent sequence. The Allan factor (AF) analysis further confirmed temporal clustering, with deviations from the theoretical Poisson process observed in most models, particularly Reasenberg, which showed the most pronounced deviations, indicative of burst-like earthquake occurrences. In contrast, Uhrhammer displayed a smoother AF trend, suggesting a closer approximation to a Poisson process, a result also consistent with Benali et al. In spatial clustering analysis, the Morisita index (Iδ) and its scaling behavior highlighted variations in clustering intensity among the different declustering methods. Uhrhammer exhibited the strongest clustering behavior, as evidenced by the steepest slope of the log-log regression ($S2 = -0.27$), while Gruenthal demonstrated the weakest clustering ($S2 = -0.19$). Gardner and Knopoff ($S2 = -0.22$) and Reasenberg ($S2 = -0.23$) showed intermediate clustering levels. These observations are consistent with Benali et al., who reported similar spatial clustering persistence across different

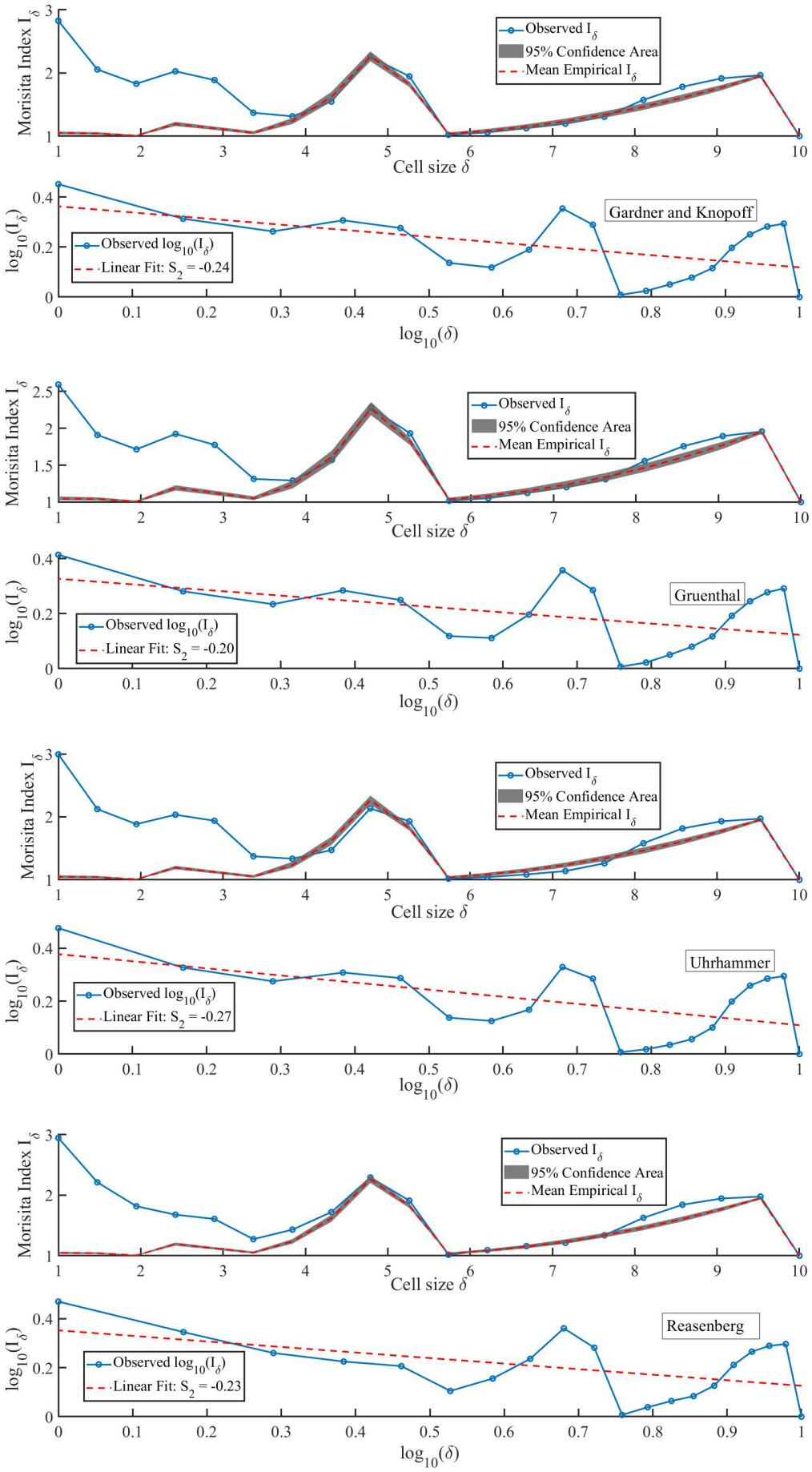

Figure 10. Empirical Morisita index measure with 95%confidence area.

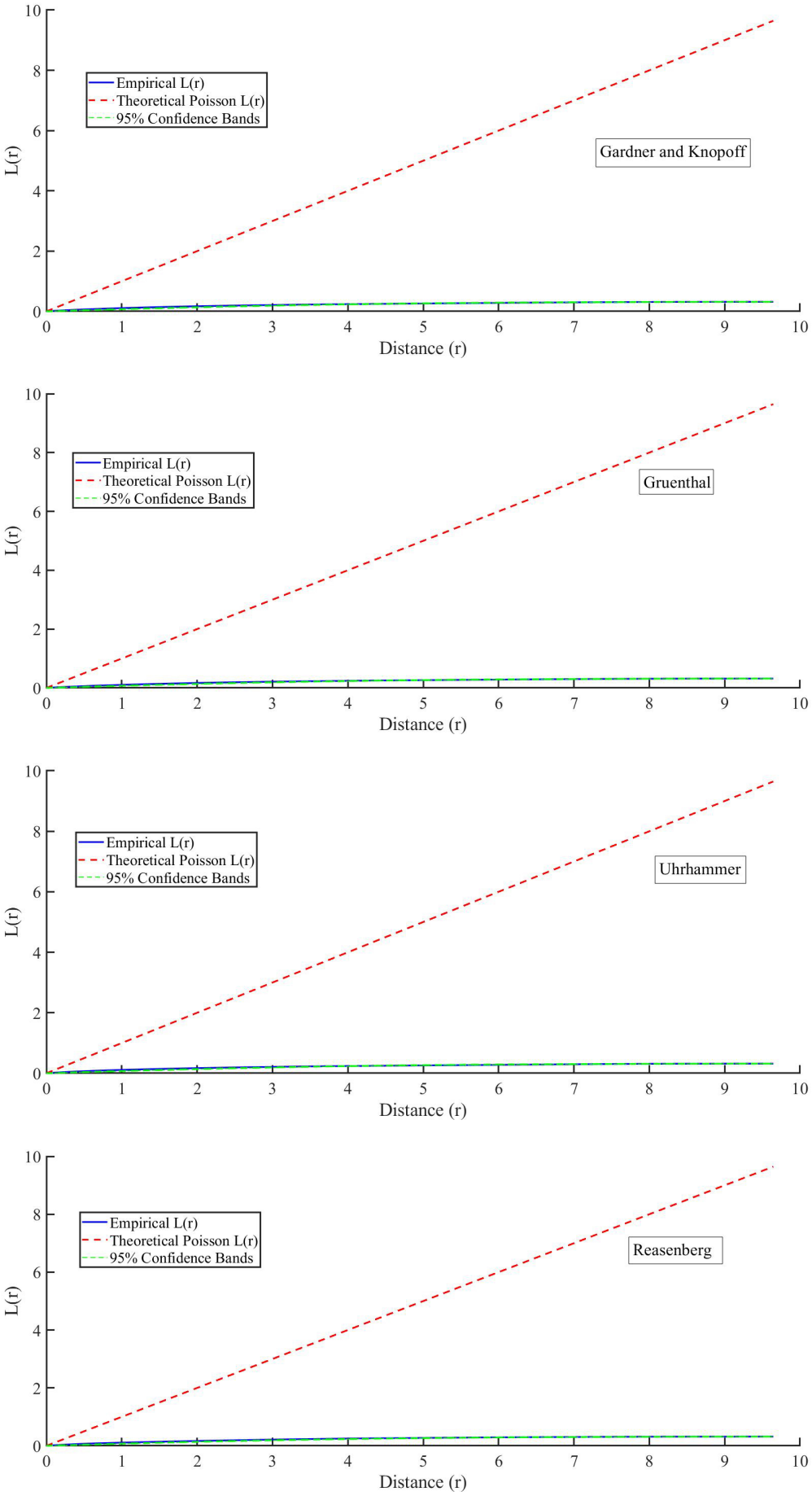

Figure 11. Inhomogeneous L function including its 95% simulation envelopes.

declustering methods. The Morisita index plots further reinforced these trends, with Reasenberg and Uhrhammer showing localized clustering, whereas Gruenthal maintained relatively stable values across different spatial scales.

The results challenge the assumption of a temporally homogeneous Poisson process, as the CV values exceeding 1, the Allan factor deviations and the spatial clustering detected by the Morisita index indicate that declustering does not eliminate clustering behavior. The degree of residual clustering varies by method, with Reasenberg preserving significant clustering, while Uhrhammer provides the closest approximation to a time-homogeneous Poisson process. These findings align with Benali et al. (2023), who also noted that different declustering approaches yield varying levels of clustering persistence. Given these observations, additional statistical tests, such as Monte Carlo simulations and likelihood-based approaches, may be required to further assess the Poissonian behavior of declustered earthquake sequences. Future research should explore alternative declustering techniques and evaluate their effectiveness in reducing clustering artifacts while maintaining the statistical properties of earthquake catalogs.

6. Conclusions

This study evaluates and compares four prominent declustering methods – Gardner-Knopoff, Gruenthal, Reasenberg, and Uhrhammer applied to seismic data from the Kathmandu Valley. The analysis of temporal clustering using the Coefficient of Variation (CV) and Allan Factor (AF) confirms that earthquake sequences retain clustering characteristics even after declustering, with Reasenberg exhibiting the highest residual clustering and Gruenthal the least. These results align with previous studies, reinforcing the persistence of temporal correlations. The spatial clustering analysis, based on the Morisita index and its scaling behavior, further reveals variations in clustering intensity across declustering methods. Uhrhammer retains the highest degree of spatial clustering, whereas Gruenthal produces the most homogeneous spatial distribution. These findings highlight that different declustering techniques yield varying levels of residual clustering, impacting the statistical properties of earthquake catalogs. Additionally, the L-function analysis with Monte Carlo simulations confirms that none of the declustered catalogs perfectly conform to a homogeneous Poisson process, with p-values of zero for all methods. This suggests that declustering does not entirely remove clustering artifacts, emphasizing the need for careful selection of declustering approaches depending on the intended application in seismic hazard analysis. This comparative study underscores the complexities of declustering seismic catalogs and the limitations of existing methods in achieving complete statistical independence. Future research should explore alternative declustering techniques and refine statistical models to better capture the true nature of earthquake sequences in complex tectonic regions like the Kathmandu Valley.

Data availability statement. The data underlying this article is available on online platforms.

Acknowledgements. The seismic event data used in this study were obtained from the United States Geological Survey (USGS), the Incorporated Research Institutions for Seismology (IRIS), and the International Seismological Centre (ISC). Their efforts in making seismic data publicly available are greatly appreciated.

References

Amini, H. (2014). Comparing Reasenberg and Gruenthal Declustering Methods for North of Iran, in Second European Conference on Earthquakes Engineering and Seismology, Istanbul AUG, 1-7.

Ansari, A. et al. (2022). Seismic hazard assessment studies based on deterministic and probabilistic approaches for the Jammu region, NW Himalayas, Arab. J. Geosci., 15, 11, 2081, doi:10.1007/s12517-022-10330-z.

Benali, A., A. Jalilian, A. Peresan, E. Varini et al. (2023). Spatiotemporal Analysis of the Background Seismicity Identified by Different Declustering Methods in Northern Algeria and Its Vicinity, Axioms, 12, 3, 1-27, doi:10.3390/axioms12030237.

Bhusal, B. and H. R. Parajuli (2019). Probabilistic Seismic Hazard Analysis for Nepal Using Areal and Longitudinal Faults Source, in Proceddings of IOE Graduate Conference, pp. 125-132.

Das, R., H. R. Wason and M. L. Sharma (2012). Temporal and spatial variations in the magnitude of completeness for homogenized moment magnitude catalogue for northeast India, J. Earth Syst. Sci., 121, 1, 19-28, doi:10.1007/s12040-012-0144-3.

Juellyan, J. B., M. Hasan, H. Yunita, M. Sungkar et al. (2023). Comparing Gardner-Knopoff, Gruenthal, and Uhrhammer Earthquake Declustering Methods in Aceh, Indonesia, in IOP Conference Series: Earth Environ. Sci., doi:10.1088/1755-1315/1245/1/012010.

Khurram, S. and P. Khalid (2022). Comparison of Different Declustering Procedures Using Pakistan Earthquake Dataset, The Geological Bulletin of the Punjab University, 55-62.

Moklesur, R., Md and L. Bai (2018). Probabilistic seismic hazard assessment of Nepal using multiple seismic source models, Earth Planet., 2, 4, 327-341, 10.26464/epp2018030.

Parajuli, H. R., B. Bhusal and S. Paudel (2021). Seismic zonation of Nepal using probabilistic seismic hazard analysis, Arab. J. Geosci., 14, 20, doi:10.1007/s12517-021-08475-4.

Poudyal, D., N. Nordin, S. Roslan, B. K. Dahal et al. (2024). Spatial Mapping of Seismic Vulnerability Index in Kathmandu Valley: Insight from Dominant Frequency and Amplification Factor, J. Geophys. Eng., 1272-1285. doi:10.1093/jge/gxae069.

Pradhan, P. M., S. P. Timalsinaand and M. R. Bhatt (2020). Probabilistic seismic hazard analysis for Nepal, Lowl. Technol. Int., 22(1), 75-80, doi:10.3126/jiee.v2i1.36676.

Pramono, S., W. A. Prakoso, S. Rohadi, D. Karnawati et al.(2020) Influence of seismicity declustering on ground motion prediction equations for central sulawesi seismic region, Int. J. GEOMATE, 19, 71, 61-68, doi:10.21660/2020.71.28369.

Rahman, M. M., L. Bai, N. G. Khan, Li Guohui et al. (2018). Probabilistic Seismic Hazard Assessment for Himalayan-Tibetan Region from Historical and Instrumental Earthquake Catalogs, Pure Appl. Geophys., 175, 2, 685-705, doi:10.1007/s00024-017-1659-y.

Risanti, H., A. Realita, M. N. Fahmi, T. Prastowo and M. Madlazim (2022). A preliminary report on seismicity declustering methods and completeness magnitude in eastern Sunda Arc, J. Phys.: Conference Series, 2377, 1, doi:10.1088/1742-6596/2377/1/012033.

Van Stiphout, T., J. Zhuang and D. Marsan(2012). Models and Techniques for Analyzing Seismicity declustering, Community Online Resource for Statistical Seismicity Analysis, 1, 1-25, doi:10.5078/corssa-52382934.

Utsu, T., Y. Ogata and R. S. Matsura (1995). The centenary of the omori formula for a decay law of aftershock activity, J. Phys. Earth, 43, 1, 1-33, doi:10.4294/jpe1952.43.1.

Wiemer, S. (2001). A software package to analyze seismicity: ZMAP, Seismol. Res. Lett., 72, 3, 373-382, doi:10.1785/gssrl.72.3.373.

Wyss, M., S. Wiemer and R. Zúñiga (2001). Zmap a Tool for Analyses of Seismicity Patterns Typical Applications and Uses, Writing, 64.

***CORRESPONDING AUTHOR: Dibyashree POUDYAL**,
Department of Civil Engineering, Infrastructure University Kuala Lumpur, De Centrum City, Jalan Ikram-Uniten, 43000 Kajang, Selangor, Malaysia
e-mail: 082101900007@s.iukl.edu.my